

Efficient Dynamic Scene Editing via 4D Gaussian-based Static-Dynamic Separation

JooHyun Kwon*
DGIST, South Korea
rnjswngus00.dgist.ac.kr

Hanbyel Cho*
KAIST, South Korea
t1r14658@gmail.com

Junmo Kim
KAIST, South Korea
junmo.kim@kaist.ac.kr

Abstract

Recent 4D dynamic scene editing methods require editing thousands of 2D images used for dynamic scene synthesis and updating the entire scene with additional training loops, resulting in several hours of processing to edit a single dynamic scene. Therefore, these methods are not scalable with respect to the temporal dimension of the dynamic scene (i.e., the number of timesteps). In this work, we propose an efficient dynamic scene editing method that is more scalable in terms of temporal dimension. To achieve computational efficiency, we leverage a 4D Gaussian representation that models a 4D dynamic scene by combining static 3D Gaussians with a Hexplane-based deformation field, which handles dynamic information. We then perform editing solely on the static 3D Gaussians, which is the minimal but sufficient component required for visual editing. To resolve the misalignment between the edited 3D Gaussians and the deformation field potentially resulting from the editing process, we additionally conducted a refinement stage using a score distillation mechanism. Extensive editing results demonstrate that our method is efficient, reducing editing time by more than half compared to existing methods, while achieving high editing quality that better follows user instructions.

1. Introduction

Diffusion-based generative models [10, 20, 40, 44, 46, 47, 65] have recently achieved remarkable advancements in the 2D image domain and are increasingly being adopted in practical applications. As demand grows for generative tasks beyond 2D, the editing of 3D and 4D dynamic scenes is emerging as a significant research focus. Notably, user instruction-guided editing is gaining attention as a highly user-friendly approach.

In this context, InstructPix2Pix (IP2P) [4] has gained recognition by proposing a novel method for editing 2D

*Equal contribution.

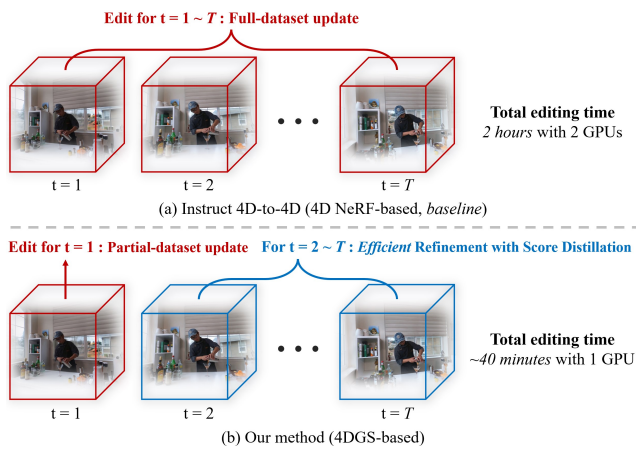


Figure 1. **Illustration of dynamic scene editing processes for baseline and our method:** (a) The existing method requires updating the 2D images relevant to all timesteps. (b) In contrast, our method updates only the first timestep’s dataset images, editing canonical 3D Gaussians and completing dynamic scene editing efficiently through score-based temporal refinement. For a multi-camera dataset with $T = 300$, our method reduces editing time by more than half compared to the baseline, using only a single GPU.

images based on user instructions. Building on IP2P’s capabilities, research exploring instruction-guided 3D scene editing based on NeRF [36] and 3D Gaussian Splatting (3DGS) [23] has become increasingly active. However, research on 4D dynamic scene editing remains relatively underexplored. One of the few existing methods, Instruct 4D-to-4D [37] requires iterative dataset updates for “thousands of 2D images” used in the dynamic scene synthesis, as shown in Fig. 1 (a), along with additional training loops to update the entire dynamic scene, resulting in several hours of processing to edit a single dynamic scene. No matter how efficiently the dataset update is performed, such a method is not scalable with respect to the temporal dimension of dynamic scenes, making it impractical for real-world applications.

In this work, we propose an efficient 4D dynamic scene editing method that is more scalable for its temporal dimen-

sion. To maximize computational efficiency, we focus on three key aspects: (1) Since 4D dynamic scenes require frequent rendering during the editing process, we employ 4D Gaussian Splatting (4DGS) [60] to leverage a 4D dynamic scene representation, which enables fast and efficient rendering. (2) Our goal is to edit the appearance of the scene rather than its motion. Thus, we focus on the separability of 4DGS into static component (*i.e.*, canonical 3D Gaussians) and dynamic components (*i.e.*, Hexplane [5, 15]-based deformation field), achieving editing efficiency by editing only the static component. (3) To better align the edited static 3D Gaussians with the original deformation field, we perform temporal refinement using a score distillation mechanism [41].

Specifically, the Hexplane-based 4DGS offers notable advantages in editing quality and rendering efficiency compared to the 4D NeRF [52] adopted in Instruct 4D-to-4D. By using 3D Gaussians as the representation of the static canonical scene, we ensure high-quality real-time rendering during the editing process. Hexplane, which utilizes a spatio-temporal encoding structure based on planar factorization, is also compact and contributes to real-time rendering performance.

In addition to rendering efficiency, we aim to achieve computational efficiency in dynamic scene editing by proposing a method that edits only the static component. Our goal is to edit the scene’s appearance rather than its motion, so we focus solely on editing the static 3D Gaussians, which is the minimal yet sufficient elements required for appearance editing. As shown in Fig. 1 (b), this approach allows us to edit the entire dynamic scene without updating every 2D image, even for dynamic scenes with extended timesteps. Specifically, we edit only a subset of 2D multiview images corresponding to the initial timestep using IP2P and then apply simple edits to the static 3D Gaussians through L1 RGB loss.

While editing only the static 3D Gaussians is simple and efficient, it introduces motion artifacts in the later timesteps. Specifically, during the editing of static 3D Gaussians, the positions of Gaussian primitives shift slightly, causing the static canonical scene to deviate from the original deformation field. Additionally, only the Spherical Harmonics (SH) colors of the 3D Gaussians visible in the first timestep are updated. Consequently, if the Gaussian primitives rotate through the deformation field in subsequent timesteps, the un-updated SH values become exposed, leading to visual artifacts. In summary, the dynamic scene tends to overfit to the first timestep, resulting in visual artifacts across other timesteps.

To improve this temporal misalignment, we propose a refinement stage that adjusts the edited static 3D Gaussians to align with the original deformation fields. For this purpose, we utilize the score distillation mechanism pro-

posed in DreamFusion [41] to transfer the editing guidance of IP2P into 3D and even 4D spaces. Specifically, we applied a score-based refinement stage to eliminate artifacts in the *pseudo-edited dynamic scene* (*i.e.*, the edited static 3D Gaussians misaligned with the deformation field). In addition, we replaced the self-attention module of IP2P with a cross-attention module, inspired by MVDream [50] and Tune-a-Video [61]. This modified IP2P, Coherent-IP2P contributes to preventing the accumulation of non-uniform editing guidance during the score distillation process, which would otherwise result in blurry outputs.

The evaluation shows a significant reduction in the editing turnaround time of our method along with improved visual quality. Additionally, our method can effectively perform dynamic scene editing across various input instructions. Our main contributions are summarized as follows:

- We introduce the first efficient dynamic scene editing framework based on 4D Gaussian Splatting.
- To achieve efficient dynamic scene editing, we propose a method that edits only static 3D Gaussians, which is the minimal but sufficient component for visual editing.
- We propose a refinement method that utilizes a score distillation mechanism using Coherent-IP2P to remove motion artifacts while maintaining the computational efficiency of dynamic scene editing.
- Experimental results show that our method can reduce the editing time by more than half with better quality.

2. Related Work

2.1. 4D Dynamic Scene Representation

Recent advancements in computer vision and graphics have driven interest in 4D dynamic scene representation, which models both spatial and temporal information. As methods for capturing high-quality 4D content have advanced, multi-view 4D data has become increasingly available, emphasizing the need for efficient representations to address high computational costs in 4D modeling. Many approaches [12, 33, 39, 42, 48, 52, 56] have reduced the complexity of dynamic scene representation by handling the temporal dimension separately, resulting in the decoupling of the canonical 3D representation and the deformation field. Specifically, K-plane and Hexplane [5, 15] construct spatio-temporal encoding structures in the deformation field using multi-scale parameter grids through planar factorization. On the other hand, other works [13, 29, 30, 63] have enhanced the overall performance of dynamic scenes by employing 3D Gaussian Splatting [23] as the canonical 3D representation, which has recently gained attention for its real-time rendering capabilities and high quality. Notably, 4D Gaussian Splatting [60] combines 3DGS with the Hexplane deformation field to achieve real-time

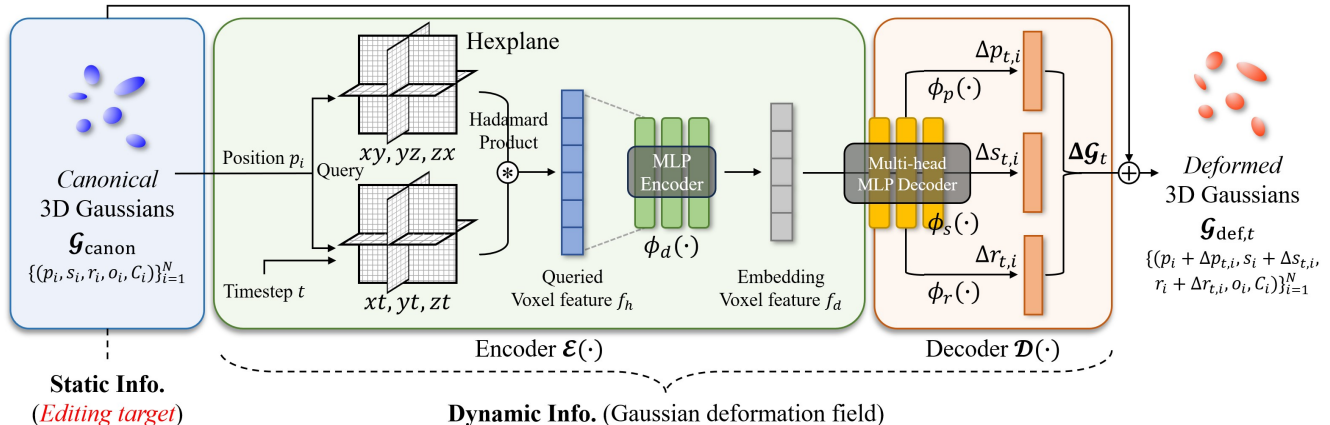


Figure 2. **Overview of 4D Gaussian Splatting:** The 4DGS represents dynamic scenes by separating static component (canonical 3D Gaussians $\mathcal{G}_{\text{canon}}$) and dynamic components (Gaussian deformation field $\{\mathcal{E}(\cdot), \mathcal{D}(\cdot)\}$). A spatio-temporal embedding voxel feature f_d is queried from the Hexplane using each Gaussian primitive’s position p and timestep t . This feature is then processed through a multi-head MLP decoder $\{\phi_p(\cdot), \phi_s(\cdot), \phi_r(\cdot)\}$ to produce per-Gaussian deformation $\Delta p_{t,i}$, $\Delta s_{t,i}$ and $\Delta r_{t,i}$, which are added to the canonical 3D Gaussians to generate deformed Gaussians $\mathcal{G}_{\text{def},t}$. By repeatedly generating $\mathcal{G}_{\text{def},t}$ and rendering them across a sequence of timesteps, a video output can be obtained from the dynamic scene.

rendering speeds and more accurately model the dynamic scenes. Owing to its excellent performance, 4DGS has significant potential for tasks such as dynamic scene generation [1, 32, 45], editing [37, 49], and tracking [16, 35]. In this paper, we employ 4DGS to maximize the efficiency of the dynamic scene editing process.

2.2. Instruction-Guided Scene Editing

User instructions provide one of the most user-friendly approaches to scene editing. InstructPix2Pix [4] introduced the task of instruction-guided editing by fine-tuning the Stable Diffusion [46] model on a dataset comprising *source image–instruction–target image* triplets. Recent studies [7, 8, 11, 17, 22, 62] have extended IP2P’s capabilities to 3D scenes by developing methods to ensure spatial consistency in editing guidance, thereby making significant progress in instruction-guided 3D scene editing despite the limited availability of 3D datasets. One of the key trends among these approaches is the iterative dataset update method, which involves editing all the 2D images used for 3D scene synthesis, followed by re-training the 3D scene. Recently, Instruct 4D-to-4D [37] extended the iterative dataset update approach to 4D space, presenting the first instruction-guided 4D editing method. By employing flow-based warping [55] and depth-based warping to ensure spatio-temporal consistency during dataset updates, they achieved notable results. However, editing all images for 4D dynamic scenes remains extremely time-consuming, highlighting the need for a method that can efficiently utilize diffusion priors for dynamic scene editing. Therefore, we propose an efficient dynamic scene editing method that can significantly reduce total editing time.

2.3. Score Distillation Sampling

The Score Distillation Sampling (SDS) mechanism was introduced in DreamFusion [41] for text-to-3D scene generation, providing a path to transfer the priors of pre-trained 2D diffusion models [4, 20, 46] to other data domains. When SDS is used with diffusion networks incorporating specific hypotheses—such as multiview diffusion models [50, 57] or video diffusion models [2, 3, 21, 34, 51, 61]—it can produce guidance that aligns with those specific hypotheses. Many studies [1, 31, 32, 41, 45, 54, 64] have leveraged this property to propose SDS-based 3D/4D generation tasks. On the other hand, some approaches [9, 22, 28, 59, 62, 67] have applied SDS to editing tasks. Additionally, works like [18, 24, 26] have contributed to improving editing performance by modifying the score loss function to suit the editing task better.

3. Preliminary

For efficient dynamic scene editing, we utilize a 4D Gaussian Splatting (4DGS) [60] that represents the scene by separating static and dynamic information. In this section, we present a brief overview of the 4DGS focusing especially on its Hexplane [5, 15]-based Gaussian deformation field, followed by an explanation of the proposed method in Sec. 4.

4D Gaussian Splatting. 4DGS consists of a canonical 3D Gaussians [23] $\mathcal{G}_{\text{canon}}$ that represents static information and a Gaussian deformation field that represents dynamic information and produces each Gaussian’s deformation $\Delta \mathcal{G}_t$ (where t is a normalized value from 0 to 1, denoting the timestep within the dynamic scene), as illus-

trated in Fig. 2. The 3D Gaussians $\mathcal{G}_{\text{canon}}$ representing the undeformed static canonical 3D scene consist of N Gaussian primitives (in our case, $N = 100k\text{--}200k$), denoted as $\mathcal{G}_{\text{canon}} = \{(p_i, s_i, r_i, o_i, C_i)\}_{i=1}^N$, where each primitive is defined by a position $p \in \mathbb{R}^3$, a scaling vector $s \in \mathbb{R}^3$, a rotation quaternion $r \in \mathbb{R}^4$, an opacity $o \in \mathbb{R}$, and a spherical harmonics color $C \in \mathbb{R}^k$, with k determined by the SH degree. The Gaussian deformation field $\{\mathcal{E}(\mathcal{G}_{\text{canon}}, t), \mathcal{D}\}$ is composed of an encoder part $\mathcal{E}(\mathcal{G}_{\text{canon}}, t)$, which outputs an embedding voxel feature f_d based on spatio-temporal input coordinates p and t , and a decoder part \mathcal{D} , which decodes the voxel feature into the each Gaussian’s deformation $\Delta\mathcal{G}_t$. Note that, to ensure Gaussian deformations resemble real-world physical motion, 4DGS computes deformation values only for Gaussian position p , scale s , and rotation r . Therefore, $\Delta\mathcal{G}_t$ can be expressed as $\{\Delta p_{t,i}, \Delta s_{t,i}, \Delta r_{t,i}\}_{i=1}^N$. By repeatedly adding the outputs of the deformation field $\Delta\mathcal{G}_t = \mathcal{D}(\mathcal{E}(\mathcal{G}_{\text{canon}}, t))$ to the canonical 3D Gaussians $\mathcal{G}_{\text{canon}}$ at each timestep t , we can render an image $\hat{I}_{M,t}$ from deformed 3D Gaussians $\mathcal{G}_{\text{def},t} = \mathcal{G}_{\text{canon}} + \Delta\mathcal{G}_t$ as: $\hat{I}_{M,t} = S(M, \mathcal{G}_{\text{def},t})$, where M denotes the camera matrix, and S represents the rendering (differential splatting) process of the 3DGS.

Encoder for Gaussian Deformation Field. 4DGS incorporates Hexplane [5, 15], as a core component in the structure of the encoder $\mathcal{E}(\mathcal{G}_{\text{canon}}, t)$ within its Gaussian deformation field. The Hexplane is a spatio-temporal structure encoder and can be viewed as a generalization of Triplane [6], which was originally designed to embed spatial information in 3D space.

Hexplane-based encoder $\mathcal{E}(\mathcal{G}_{\text{canon}}, t)$ can be parametrized by six multi-resolution voxel grids R_l across the four dimensions (x, y, z, t) and simple MLP encoder ϕ_d as $\mathcal{E}(\mathcal{G}_{\text{canon}}, t) = \{R_l(i, j), \phi_d(i, j) \in \{(x, y), (y, z), (x, z), (x, t), (y, t), (z, t)\}, l \in \{1, 2\}\}$, where l represents the multi-resolution level (the multi-resolution technique is relevant to Instant-NGP [38], enabling fast optimization and rendering).

The spatio-temporal embedding voxel feature f_d is obtained from the Hexplane as $f_d = \phi_d(f_h)$, where $f_h = \bigcup_l \prod \text{interp}(R_l(i, j))$, and $(i, j) \in \{(x, y), (x, z), (y, z), (x, t), (y, t), (z, t)\}$. In 4DGS, the x, y , and z coordinates of the Gaussian position p and timestep t is used to query voxel features across six planes. The six voxel features obtained from each plane through bilinear interpolation are then combined via the Hadamard product (channel-wise product). This queried voxel feature f_h is subsequently passed through ϕ_d to yield the final embedding voxel feature f_d as shown in Fig. 2.

Decoder for Gaussian Deformation Field. The spatio-temporal voxel feature f_d passes through a multi-head simple MLP decoder $\mathcal{D} = \{\phi_p, \phi_s, \phi_r\}$, which decodes it into

the deformation values of the Gaussian feature p, s and r as $\Delta p = \phi_p(f_d)$, $\Delta s = \phi_s(f_d)$, and $\Delta r = \phi_r(f_d)$.

Since the entire deformation field $\{\mathcal{E}(\mathcal{G}_{\text{canon}}, t), \mathcal{D}\}$ is designed with a compact Hexplane and a simple MLP, 4DGS achieves real-time rendering speeds. This provides a significant advantage for editing tasks, where rendering is performed frequently. To leverage this efficiency and the static-dynamic separability, we applied 4DGS to our primary representation for 4D dynamic scenes.

4. Method

In this section, we explain our efficient dynamic scene editing method illustrated in Fig. 3. (Sec. 4.1) We first train dynamic scenes for editing targets by optimizing the 4D Gaussian Splatting (4DGS) [60]. (Sec. 4.2) Motivated by the static-dynamic separability of Hexplane [5, 15]-based 4DGS, we initially focus on editing the static canonical 3D Gaussians [23] to efficiently edit the dynamic scene. (Sec. 4.3) To mitigate overfitting issues that may arise during the 3D Gaussian editing process and refine the motion artifacts in the dynamic scene, we introduce a temporal refinement stage using score distillation.

4.1. Optimizing 4D Gaussians for Target Scenes

To perform editing, we first require the 4D Gaussian representation of the target dynamic scene. To obtain this, we optimize the 4D Gaussians and use it for editing. Specifically, we use a dynamic scene dataset [27] composed of multi-camera captured videos, which can be represented as a set of images $\{I_{M,t}\}$ in which M denotes the camera matrix and t denotes the timestep within the videos. We synthesize images $\hat{I}_{M,t}$ by rendering the randomly initialized dynamic scene $\{\mathcal{G}_{\text{canon}}^{\text{init}}, \mathcal{E}^{\text{init}}(\mathcal{G}_{\text{canon}}, t), \mathcal{D}^{\text{init}}\}$. Then we calculate the RGB L1 loss against the corresponding dataset image $I_{M,t}$, training the dynamic scene through this process. We also applied a grid-based total variational loss [5, 14, 15, 53], \mathcal{L}_{TV} to ensure smoothness in the deformation field output along the timesteps. Note that, as our editing method is highly dependent on the quality of the target dynamic scene, incorporating such regularization loss is helpful. The entire loss function used for 4DGS training is: $\mathcal{L}_{\text{4DGS}} = |\hat{I}_{M,t} - I_{M,t}| + \mathcal{L}_{\text{TV}}$.

As a result, we obtain the optimized 4D Gaussians $\{\mathcal{G}_{\text{canon}}^{\text{opt}}, \mathcal{E}^{\text{opt}}(\mathcal{G}_{\text{canon}}, t), \mathcal{D}^{\text{opt}}\}$, which represent the editing target dynamic scene. The static component $\mathcal{G}_{\text{canon}}^{\text{opt}}$ serves as the main editing target in Sec. 4.2 to Sec. 4.3. To resolve the misalignment between the edited static component $\mathcal{G}_{\text{canon}}^{\text{edit}}$ and the dynamic components $\{\mathcal{E}^{\text{opt}}(\mathcal{G}_{\text{canon}}, t), \mathcal{D}^{\text{opt}}\}$, we apply score [41]-based temporal refinement in Sec. 4.3. A more detailed training setup follows [60].

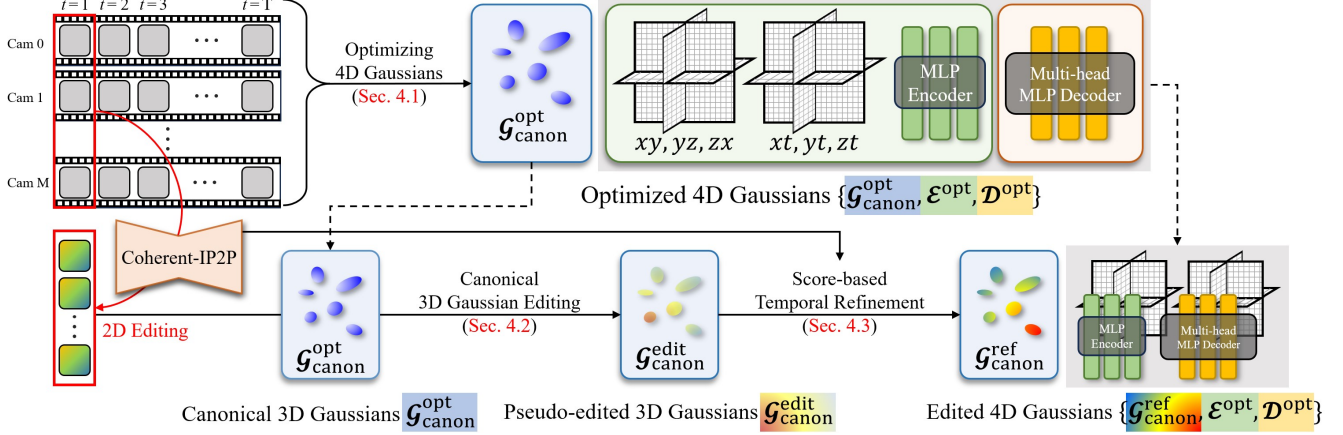


Figure 3. **Overall pipeline of our proposed dynamic scene editing method:** To obtain the target dynamic scene for editing, we first optimize the 4D Gaussians using a multi-camera captured video dataset (Sec. 4.1). We then perform 3D Gaussian editing on the static canonical 3D Gaussians by editing only the multiview images corresponding to the first timestep (Sec. 4.2). We apply score-based temporal refinement to mitigate motion artifacts without additional image editing (Sec. 4.3).

4.2. Stage 1: Efficient Dynamic Scene Editing with Static 3D Gaussians

In Sec. 4.1, we obtained the optimized canonical 3D Gaussians $\mathcal{G}_{\text{canon}}^{\text{opt}}$, which models the explicit appearance and geometry of a 3D scene, along with the optimized dynamic components $\mathcal{E}^{\text{opt}}(\mathcal{G}_{\text{canon}}, t)$ and \mathcal{D}^{opt} . For efficient dynamic scene editing, we perform editing only on $\mathcal{G}_{\text{canon}}^{\text{opt}}$, which is minimal but sufficient static information for visual editing of the dynamic scene as shown in Fig. 3.

To obtain supervision images for editing the $\mathcal{G}_{\text{canon}}^{\text{opt}}$, we extract a subset of multiview images fixed at the initial timestep and edited them using InstructPix2Pix [4]. Subsequently, we edit optimized canonical 3D Gaussians $\mathcal{G}_{\text{canon}}^{\text{opt}}$ with an L1 RGB loss supervising the edited images. Compared to the latest 4D editing method Instruct 4D-to-4D [37], which requires editing (number of video timesteps $T \times$ number of cameras \mathcal{M}) images through iterative dataset updates, our approach significantly reduces the computation required to address the editing of the dynamic scene. Moreover, this approach enables fast shifts to the edited result, regardless of the number of timesteps T of the dynamic scene. After completing the 3D Gaussian editing process, we can obtain a *pseudo-edited dynamic scene* $\{\mathcal{G}_{\text{canon}}^{\text{edit}}, \mathcal{E}^{\text{opt}}(\mathcal{G}_{\text{canon}}, t), \mathcal{D}^{\text{opt}}\}$, which is obtained by simply recombining the edited canonical 3D Gaussians $\mathcal{G}_{\text{canon}}^{\text{edit}}$ with the original Gaussian deformation field $\{\mathcal{E}^{\text{opt}}(\mathcal{G}_{\text{canon}}, t), \mathcal{D}^{\text{opt}}\}$.

To ensure spatial consistency of the 3D Gaussian editing process, we utilize Coherent-IP2P [37, 50, 61], which replaces the 2D convolutional layer (self-attention module) with a 3D convolutional layer (cross-attention module), similar to Instruct 4D-to-4D (by reusing the original parameters of kernels). As shown in Fig. 8, this encourages col-

laborative editing among images within the multiview subset, preventing the results from becoming blurry. The entire editing process for the static canonical 3D Gaussian editing can be completed within a few tens of minutes by editing only multiview images of a single timestep and performing a few hundred 3DGS editing iterations.

4.3. Stage 2: Refinement using Score Distillation for Temporal Alignment

After the first editing stage proposed in Sec. 4.2, the *pseudo-edited dynamic scene* $\{\mathcal{G}_{\text{canon}}^{\text{edit}}, \mathcal{E}^{\text{opt}}(\mathcal{G}_{\text{canon}}, t), \mathcal{D}^{\text{opt}}\}$ exhibits severe motion artifacts, as shown in Fig. 4 (a). The main reason is that during the 3D Gaussian editing process, the positions p of Gaussian primitives in $\mathcal{G}_{\text{canon}}^{\text{opt}}$ shift slightly, causing the queried embedding voxel features f_h to differ from the original dynamic scene. Moreover, only the Spherical Harmonics (SH) colors on the surface visible at the initial timestep are updated. As a result, if the Gaussian primitives in *pseudo-edited* $\mathcal{G}_{\text{canon}}^{\text{edit}}$ rotate at later timesteps, unedited SH values that were previously hidden may become exposed, leading to artifacts. Therefore, we introduce a temporal refinement stage to resolve the misalignment between the original deformation field $\{\mathcal{E}^{\text{opt}}(\mathcal{G}_{\text{canon}}, t), \mathcal{D}^{\text{opt}}\}$ and the edited canonical 3D Gaussians $\mathcal{G}_{\text{canon}}^{\text{edit}}$.

To perform the refinement stage efficiently without editing additional dataset images, we employed the score distillation mechanism [41]. Since the dynamic scene is also synthesized from multiple 2D images, the prior of the 2D diffusion model can be distilled into the 4D dynamic scene representation. The editing process can be continued using the noise prediction loss (*i.e.* score) obtained from each IP2P inference as Eqs. 1 and 2. Since we just use score distillation for editing refinement rather than generation or

editing from scratch, this stage can be completed with a smaller number of iterations. Consequently, our approach is relatively less affected by inherent issues of Score Distillation Sampling (SDS), such as the *Janus problem* [50].

Similar to Sec. 4.2, we applied Coherent-IP2P with the diffusion prior θ and observed that it reduces blurring effects and enhances qualitative performance compared to the original IP2P. At each refinement iteration, we rendered B images of the *pseudo-edited dynamic scene* $\tilde{I} = \left\{ \hat{I}_i = S(M_i, \mathcal{G}_{\text{def}, t_i}^{\text{edit}} + \Delta G_{t,i}) \right\}_{i=1}^B$ using random camera matrices $\{M_i\}_{i=1}^B$ and random timesteps $\{t_i\}_{i=1}^B$ as input for Coherent-IP2P, where S denotes the rendering process of the 3DGS (subscripts M and t on \hat{I} omitted for simplicity). The SDS loss we used to obtain refined 3D Gaussians $\mathcal{G}_{\text{canon}}^{\text{ref}}$ is as follows:

$$\nabla_{\mathcal{G}_{\text{canon}}^{\text{edit}}} \mathcal{L}_{\text{SDS}} = \mathbb{E}_{t, \tilde{t}, \epsilon, \mathcal{M}} \left[\left(\epsilon_{\theta}(\tilde{I}, c_I, c_T; t, \tilde{t}, \mathcal{M}) - \epsilon \right) \frac{\partial \tilde{I}}{\partial \mathcal{G}_{\text{canon}}^{\text{edit}}} \right], \quad (1)$$

$$\begin{aligned} \epsilon_{\theta}(\tilde{I}, c_I, c_T) &= \epsilon_{\theta}(\tilde{I}, \emptyset, \emptyset) + s_I \left(\epsilon_{\theta}(\tilde{I}, c_I, \emptyset) - \epsilon_{\theta}(\tilde{I}, \emptyset, \emptyset) \right) \\ &\quad + s_T \left(\epsilon_{\theta}(\tilde{I}, c_I, c_T) - \epsilon_{\theta}(\tilde{I}, c_I, \emptyset) \right) \end{aligned} \quad (2)$$

, where \tilde{t} is diffusion timestep, ϵ is diffusion noise, $c_I = \{I_i\}_{i=1}^B$ is original dataset images, c_T is user instruction, s_I and s_T are Classifier-Free-Guidance [19] scale for c_I and c_T , $\epsilon_{\theta}(\tilde{I}, c_I, c_T)$ is Coherent-IP2P denoiser networks including VAE [25]. This score-based guidance encourages a set of rendered 2D images from the *pseudo-edited* 4D Gaussians at arbitrary timesteps \tilde{I} to resemble the edited images that IP2P would generate based on the c_I and c_T , thereby effectively refining motion artifacts. As a result, we obtain refined canonical 3D Gaussians $\mathcal{G}_{\text{canon}}^{\text{ref}}$ that aligns well with the original deformation field $\{\mathcal{E}^{\text{opt}}(\mathcal{G}_{\text{canon}}, t), \mathcal{D}^{\text{opt}}\}$ while maintaining the edited appearance. After the refinement stage, we finally obtain a completely edited 4D dynamic scene represented by 4D Gaussians as $\{\mathcal{G}_{\text{canon}}^{\text{ref}}, \mathcal{E}^{\text{opt}}(\mathcal{G}_{\text{canon}}, t), \mathcal{D}^{\text{opt}}\}$.

5. Experiments

5.1. Experimental Setup

Datasets. We utilize the real-world multiview video dataset, DyNeRF [27] to train and edit the 4D dynamic scene. The DyNeRF dataset includes six 10-second video sequences captured at 30 fps by 15 to 20 cameras with face-forward perspective. Therefore, extracting each timestep of the video as an image results in thousands of images.

Baselines. We conduct a qualitative and quantitative comparison with Instruct 4D-to-4D [37], the only prior work addressing instruction-guided 4D dynamic scene editing. Instruct 4D-to-4D utilizes NeRFPlayer [52] as its backbone



(a) Before score-based temporal refinement



(b) After score-based temporal refinement

Figure 4. Effectiveness of score-based temporal refinement: Proposed score-based temporal refinement effectively resolves the misalignment between the canonical 3D Gaussians and the original deformation field that arises during the 3D Gaussian editing process. Without requiring additional 2D image updates, this process efficiently completes the dynamic scene editing within a few hundred iterations.

4D representation and employs an iterative dataset update method, editing all 2D images used in synthesizing the dynamic scene. It utilizes optical flow-based warping [55] and depth-based warping to ensure consistency across all edited 2D images. To alleviate the time-consuming dataset update process, Instruct 4D-to-4D uses two GPUs in parallel: one for the dataset updating (*i.e.* editing) thread and the other for the dynamic scene editing thread.

Implementation Details. In Sec. 4.1, we follow the experimental settings of [60]. Throughout the experiments utilizing InstructPix2Pix [4], we set the CFG [19] scales for image condition and text instruction to 1.2 and 10.5, respectively. In the 3D Gaussian editing stage (Sec. 4.2), 800 to 1000 iterations were performed, depending on the editing style. For the score-based [41] refinement stage (Sec. 4.3), an average of 500 iterations is sufficient to successfully complete the dynamic scene editing. All experiments were conducted using a single NVIDIA A40 GPU.

5.2. Results

Quantitative Results. We measure PSNR, SSIM [58], and LPIPS [66] between the rendered images of the edited dynamic scene and the edited 2D multiview images used in the 3D Gaussian editing stage. Note that, as the temporal refinement stage can lead to an unfair evaluation of these metrics since the score loss does not provide direct supervision for the edited 2D images, we measured them by rendering the *pseudo-edited dynamic scenes* instead. To evaluate the refined dynamic scene, we measure CLIP [43] similarity to evaluate how well the input instruction was followed. Note that, the refined dynamic scenes exhibit a higher CLIP similarity compared to the *pseudo-edited dynamic scenes*.

| Instruction | Method | PSNR \uparrow | SSIM \uparrow | LPIPS $_{VGG}\downarrow$ | CLIP sim. \uparrow |
|------------------------|--------|-----------------|-----------------|--------------------------|----------------------|
| <i>Roman Sculpture</i> | I4D24D | 24.24 | 0.865 | 0.372 | 0.229 |
| | Ours | 27.68 | 0.876 | 0.258 | 0.262 |
| <i>Statue</i> | I4D24D | 18.73 | 0.713 | 0.567 | 0.202 |
| | Ours | 28.77 | 0.882 | 0.227 | 0.225 |
| <i>Wood Sculpture</i> | I4D24D | 18.23 | 0.631 | 0.535 | 0.258 |
| | Ours | 25.20 | 0.810 | 0.264 | 0.281 |
| <i>(Average)</i> | I4D24D | 20.40 | 0.736 | 0.491 | 0.230 |
| | Ours | 27.22 | 0.856 | 0.250 | 0.256 |

Table 1. **Quantitative comparison of editing quality:** Comparison of performance metrics between Instruct 4D-to-4D (denoted as I4D24D) and our method for different instructions. Higher values are better for PSNR, SSIM, and CLIP similarity, while lower values are better for LPIPS $_{VGG}$.

| Method | Computing units | Avg. editing time |
|------------------------|-----------------|-------------------|
| Instruct 4D-to-4D [37] | 2 GPUs | 2 hours |
| Ours | 1 GPU | 40 minutes |

Table 2. **Quantitative comparison of editing efficiency:** Compared to the baseline, our method can complete dynamic scene editing in a very short time using only a single GPU, with this advantage becoming more pronounced as the number of timesteps in the dynamic scene increases.

A quantitative comparison between our method and the baseline is presented in Tab. 1. Our edited dynamic scene outperforms the baseline across all metrics, demonstrating that our method can produce higher-quality edited dynamic scenes while better following the user instruction. Tab. 2 presents the results comparing the efficiency of the baseline and the proposed method. In terms of editing time, our method completes editing 2–3 times faster than the baseline, despite using only a single GPU compared to the baseline’s use of two identical GPUs. This difference in editing time is expected to increase as the number of timesteps covered by the dynamic scene grows. These results demonstrate that the proposed method, which ensures efficiency by focusing on the static-dynamic separability of 4DGS and employing score-based temporal refinement, performs dynamic scene editing much more efficiently without the need for extensive time-consuming dataset updates.

Qualitative Results. Our qualitative results are shown in Fig. 5. Our dynamic scene editing method effectively follows various editing styles based on the provided instructions. Leveraging the capabilities of 4DGS [60], each rendered image exhibits high fidelity, accurately capturing the target details. Moreover, the rendered video output of our edited dynamic scenes maintains smooth motion.

Qualitative comparison with the baseline is in Fig. 6 and Fig. 7. As shown in the zoomed-in images of Fig. 6, our method produces a high-quality edited dynamic scene with less noise and blurry artifacts compared to the baseline. Furthermore, as shown in Fig. 7, a comparison of images across multiple timesteps from a fixed camera reveals that



Figure 5. **Qualitative results across various editing styles:** We present the editing results for the *cook_spinach*, *flame_steak*, and *coffee_martini* scenes from DyNeRF. Our method successfully generates high-quality edited dynamic scenes that closely follow the given various user instructions.

the baseline exhibits a noticeable flickering effect. These results indicate that, although the baseline attempts to ensure consistency across all 2D image edits, it falls short of achieving full temporal consistency. In comparison, our method avoids such artifacts by editing the dynamic scene across the temporal dimension through score refinement. It is worth emphasizing that these higher-quality results are achieved 2–3 times faster than the baseline.

Ablation Studies. The following ablation study explores the importance of each design choice in the proposed method, highlighting their contributions to efficiency and quality. The qualitative and user study results are in Fig. 8. We conducted a user study to evaluate the results of our ablation study. We recruited 50 random participants of varying genders and ages and collected a total of 50 preference-ranking responses on the editing quality of videos generated by the four methods mentioned in Fig. 8. As shown in the pie charts in Fig. 8, our method demonstrates the highest preference.

We first compared the results of dynamic scene editing performed solely with score-based editing, without engaging in 3D Gaussian editing (denoted as “Fully SDS”). As shown in Fig. 8, editing with only SDS loss preserved smooth motion but failed to achieve sufficient alignment with the instruction, resulting in low-fidelity output. In contrast, by using the 3D Gaussian editing stage, our method secured high fidelity while achieving effective motion refinement in the temporal refinement process without compromising fidelity or quality. This demonstrates that providing direct supervision with the edited 2D images through the 3D Gaussian editing stage is essential for ensuring editing fidelity and quality.

To mitigate inherent issues of SDS such as the *Janus*

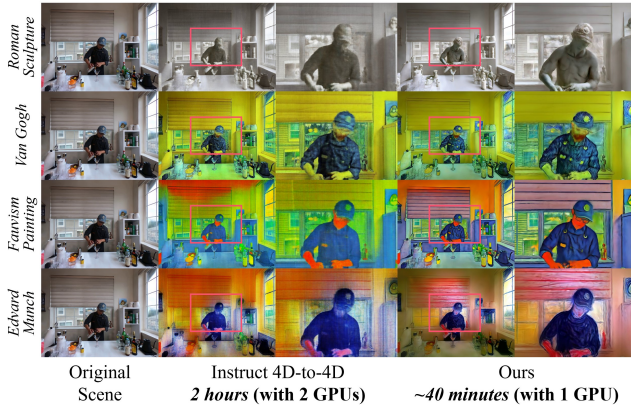


Figure 6. **Qualitative comparison of visual quality:** As shown in the zoomed-in images, the baseline exhibits blurred areas while our method produces clear results, accurately capturing fine details such as clothing folds and object contours. This demonstrates both the performance of our dynamic scene representation 4DGS and the stability of our dynamic scene editing method.

problem [50] and to obtain stable editing guidance for the score-based temporal refinement, we utilized Coherent-IP2P. To verify the effectiveness of this choice, we conducted an experiment comparing the results by refining the *pseudo-edited dynamic scene* with the original IP2P (denoted as “Refine w/ original IP2P”). Using the original IP2P for temporal refinement results in severe visual artifacts and low-quality outputs, whereas Coherent-IP2P preserves details and retains the semantics of the original scene. This demonstrates that Coherent-IP2P mitigates noisy guidance and blurry artifacts by enabling information sharing among images within the same batch.

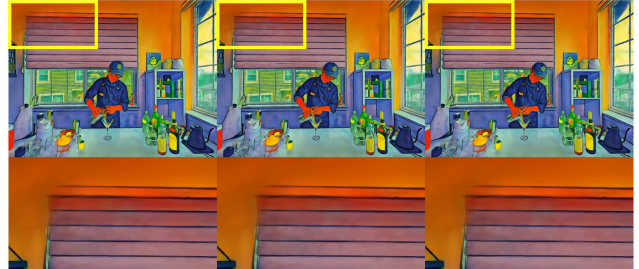
Our final method (denoted as “Ours (w/o refine $\{\mathcal{E}, \mathcal{D}\}$)”) refines only the static 3D Gaussians in the refinement stage, excluding the deformation field. This approach was chosen because refining the deformation field with Coherent-IP2P, which is not a video diffusion model, results in temporal inconsistencies and motion artifacts, as observed in “Ours (w/ refine $\{\mathcal{E}, \mathcal{D}\}$)”. (See the supplementary video file for a closer view of the qualitative results.)

6. Conclusion

Conclusion. In this work, we have proposed an efficient 4D dynamic scene editing framework leveraging 4D Gaussian Splatting (4DGS) and score distillation mechanism. Focusing on the static-dynamic separability of 4DGS, we demonstrated that editing only on the static canonical component and subsequently refining any resulting motion artifacts provides a significantly faster and more efficient approach for completing dynamic scene editing. We also showed that the score distillation mechanism can effectively transfer generative priors to 4D space, providing an efficient



(a) Instruct 4D-to-4D (baseline)



(b) Ours

Figure 7. **Qualitative comparison of temporal consistency:** As shown in the highlighted, zoomed-in areas, the baseline exhibits a flickering effect as the timestep progresses. In contrast, our method avoids such artifacts by editing only the static information and applying score-based temporal refinement.

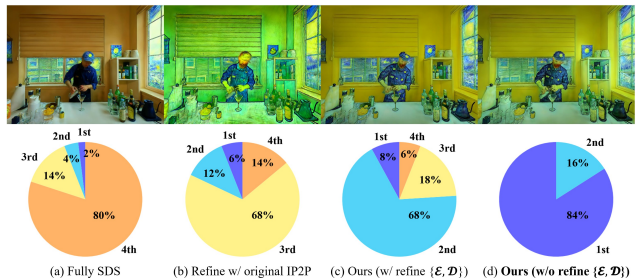


Figure 8. **Ablation study of the dynamic scene editing method:** Each segment of the pie chart represents the proportion of responses indicating the preference rank for the above result. Only the proposed method (denoted as “Ours (w/o refine $\{\mathcal{E}, \mathcal{D}\}$)”) successfully generates an appropriately edited dynamic scene, achieving the highest preference score in the user study. This demonstrates the effectiveness and validity of our dynamic scene editing method.

alternative to RGB loss, which requires additional 2D image updates. Qualitative and quantitative results have demonstrated that our method outperforms the baseline in both visual metrics and editing efficiency.

Limitations. Our method is bounded by the capabilities of IP2P; it is not suited for motion editing and requires additional segmentation pipelines for partial editing tasks. The quality of the 4D representation also imposes limitations, as it can lead to visible motion artifacts even after temporal refinement.

References

- [1] Sherwin Bahmani, Ivan Skorokhodov, Victor Rong, Gordon Wetzstein, Leonidas Guibas, Peter Wonka, Sergey Tulyakov, Jeong Joon Park, Andrea Tagliasacchi, and David B. Lindell. 4d-fy: Text-to-4d generation using hybrid score distillation sampling. *IEEE Conference on Computer Vision and Pattern Recognition (CVPR)*, 2024. [3](#)
- [2] Omer Bar-Tal, Hila Chefer, Omer Tov, Charles Herrmann, Roni Paiss, Shiran Zada, Ariel Ephrat, Junhwa Hur, Guanghui Liu, Amit Raj, Yuanzhen Li, Michael Rubinstein, Tomer Michaeli, Oliver Wang, Deqing Sun, Tali Dekel, and Inbar Mosseri. Lumiere: A space-time diffusion model for video generation, 2024. [3](#)
- [3] Andreas Blattmann, Robin Rombach, Huan Ling, Tim Dockhorn, Seung Wook Kim, Sanja Fidler, and Karsten Kreis. Align your latents: High-resolution video synthesis with latent diffusion models. In *IEEE Conference on Computer Vision and Pattern Recognition (CVPR)*, 2023. [3](#)
- [4] Tim Brooks, Aleksander Holynski, and Alexei A. Efros. Instructpix2pix: Learning to follow image editing instructions. In *Proceedings of the IEEE/CVF Conference on Computer Vision and Pattern Recognition (CVPR)*, pages 18392–18402, 2023. [1](#), [3](#), [5](#), [6](#)
- [5] Ang Cao and Justin Johnson. Hexplane: A fast representation for dynamic scenes. *CVPR*, 2023. [2](#), [3](#), [4](#)
- [6] Eric R. Chan, Connor Z. Lin, Matthew A. Chan, Koki Nagano, Boxiao Pan, Shalini De Mello, Orazio Gallo, Leonidas Guibas, Jonathan Tremblay, Sameh Khamis, Tero Karras, and Gordon Wetzstein. Efficient geometry-aware 3D generative adversarial networks. In *CVPR*, 2022. [4](#)
- [7] Minghao Chen, Iro Laina, and Andrea Vedaldi. Dge: Direct gaussian 3d editing by consistent multi-view editing. *arXiv preprint arXiv:2404.18929*, 2024. [3](#)
- [8] Yiwen Chen, Zilong Chen, Chi Zhang, Feng Wang, Xiaofeng Yang, Yikai Wang, Zhongang Cai, Lei Yang, Huaping Liu, and Guosheng Lin. Gaussianeditor: Swift and controllable 3d editing with gaussian splatting. In *Proceedings of the IEEE/CVF Conference on Computer Vision and Pattern Recognition (CVPR)*, pages 21476–21485, 2024. [3](#)
- [9] Xinhua Cheng, Tianyu Yang, Jianan Wang, Yu Li, Lei Zhang, Jian Zhang, and Li Yuan. Progressive3d: Progressively local editing for text-to-3d content creation with complex semantic prompts. In *The Twelfth International Conference on Learning Representations*, 2024. [3](#)
- [10] Sumanth Dathathri, Andrea Madotto, Janice Lan, Jane Hung, Eric Frank, Piero Molino, Jason Yosinski, and Rosanne Liu. Plug and play language models: A simple approach to controlled text generation. In *International Conference on Learning Representations*, 2020. [1](#)
- [11] Jiahua Dong and Yu-Xiong Wang. ViCA-neRF: View-consistency-aware 3d editing of neural radiance fields. In *Thirty-seventh Conference on Neural Information Processing Systems*, 2023. [3](#)
- [12] Yilun Du, Yanan Zhang, Hong-Xing Yu, Joshua B. Tenenbaum, and Jiajun Wu. Neural radiance flow for 4d view synthesis and video processing. In *Proceedings of the IEEE/CVF International Conference on Computer Vision*, 2021. [2](#)
- [13] Yuanxing Duan, Fangyin Wei, Qiyu Dai, Yuhang He, Wenzheng Chen, and Baoquan Chen. 4d-rotor gaussian splatting: Towards efficient novel view synthesis for dynamic scenes. In *Proc. SIGGRAPH*, 2024. [2](#)
- [14] Jiemin Fang, Taoran Yi, Xinggang Wang, Lingxi Xie, Xiaopeng Zhang, Wenyu Liu, Matthias Nießner, and Qi Tian. Fast dynamic radiance fields with time-aware neural voxels. In *SIGGRAPH Asia 2022 Conference Papers*, New York, NY, USA, 2022. Association for Computing Machinery. [4](#)
- [15] Sara Fridovich-Keil, Giacomo Meanti, Frederik Rahbæk Warburg, Benjamin Recht, and Angjoo Kanazawa. K-planes: Explicit radiance fields in space, time, and appearance. In *CVPR*, 2023. [2](#), [3](#), [4](#)
- [16] Zhiyang Guo, Wengang Zhou, Li Li, Min Wang, and Houqiang Li. Motion-aware 3d gaussian splatting for efficient dynamic scene reconstruction, 2024. [3](#)
- [17] Ayaan Haque, Matthew Tancik, Alexei Efros, Aleksander Holynski, and Angjoo Kanazawa. Instruct-nerf2nerf: Editing 3d scenes with instructions. In *Proceedings of the IEEE/CVF International Conference on Computer Vision*, 2023. [3](#)
- [18] Amir Hertz, Kfir Aberman, and Daniel Cohen-Or. Delta denoising score. In *Proceedings of the IEEE/CVF International Conference on Computer Vision (ICCV)*, pages 2328–2337, 2023. [3](#)
- [19] Jonathan Ho and Tim Salimans. Classifier-free diffusion guidance, 2022. [6](#)
- [20] Jonathan Ho, Ajay Jain, and Pieter Abbeel. Denoising diffusion probabilistic models. *CoRR*, abs/2006.11239, 2020. [1](#), [3](#)
- [21] Jonathan Ho, Tim Salimans, Alexey Gritsenko, William Chan, Mohammad Norouzi, and David J Fleet. Video diffusion models. *arXiv:2204.03458*, 2022. [3](#)
- [22] Hironichi Kamata, Yuiko Sakuma, Akio Hayakawa, Masato Ishii, and Takuya Narihira. Instruct 3d-to-3d: Text instruction guided 3d-to-3d conversion. *arXiv preprint arXiv:2303.15780*, 2023. [3](#)
- [23] Bernhard Kerbl, Georgios Kopanas, Thomas Leimkühler, and George Drettakis. 3d gaussian splatting for real-time radiance field rendering. *ACM Transactions on Graphics*, 42(4), 2023. [1](#), [2](#), [3](#), [4](#)
- [24] Subin Kim, Kyungmin Lee, June Suk Choi, Jongheon Jeong, Kihyuk Sohn, and Jinwoo Shin. Collaborative score distillation for consistent visual editing. In *Advances in Neural Information Processing Systems*, 2023. [3](#)
- [25] Diederik P Kingma and Max Welling. Auto-encoding variational bayes, 2022. [6](#)
- [26] Juil Koo, Chanho Park, and Minhyuk Sung. Posterior distillation sampling. In *CVPR*, 2024. [3](#)
- [27] Tianye Li, Mira Slavcheva, Michael Zollhöfer, Simon Green, Christoph Lassner, Changil Kim, Tanner Schmidt, Steven Lovegrove, Michael Goesele, Richard Newcombe, and Zhaoyang Lv. Neural 3d video synthesis from multi-view video. In *Proceedings of the IEEE/CVF Conference on Computer Vision and Pattern Recognition (CVPR)*, pages 5521–5531, 2022. [4](#), [6](#)

- [28] Yuhan Li, Yishun Dou, Yue Shi, Yu Lei, Xuanhong Chen, Yi Zhang, Peng Zhou, and Bingbing Ni. Focaldreamer: Text-driven 3d editing via focal-fusion assembly, 2023. [3](#)
- [29] Zhan Li, Zhang Chen, Zhong Li, and Yi Xu. Spacetime gaussian feature splatting for real-time dynamic view synthesis. In *Proceedings of the IEEE/CVF Conference on Computer Vision and Pattern Recognition (CVPR)*, pages 8508–8520, 2024. [2](#)
- [30] Yiqing Liang, Numair Khan, Zhengqin Li, Thu Nguyen-Phuoc, Douglas Lanman, James Tompkin, and Lei Xiao. Gaufré: Gaussian deformation fields for real-time dynamic novel view synthesis, 2023. [2](#)
- [31] Chen-Hsuan Lin, Jun Gao, Luming Tang, Towaki Takikawa, Xiaohui Zeng, Xun Huang, Karsten Kreis, Sanja Fidler, Ming-Yu Liu, and Tsung-Yi Lin. Magic3d: High-resolution text-to-3d content creation. In *IEEE Conference on Computer Vision and Pattern Recognition (CVPR)*, 2023. [3](#)
- [32] Huan Ling, Seung Wook Kim, Antonio Torralba, Sanja Fidler, and Karsten Kreis. Align your gaussians: Text-to-4d with dynamic 3d gaussians and composed diffusion models. In *Proceedings of the IEEE/CVF Conference on Computer Vision and Pattern Recognition (CVPR)*, pages 8576–8588, 2024. [3](#)
- [33] Jia-Wei Liu, Yan-Pei Cao, Weijia Mao, Wenqiao Zhang, David Junhao Zhang, Jussi Keppo, Ying Shan, Xiaohu Qie, and Mike Zheng Shou. Devrf: Fast deformable voxel radiance fields for dynamic scenes. *arXiv preprint arXiv:2205.15723*, 2022. [2](#)
- [34] Yixin Liu, Kai Zhang, Yuan Li, Zhiling Yan, Chujie Gao, Ruoxi Chen, Zhengqing Yuan, Yue Huang, Hanchi Sun, Jianfeng Gao, Lifang He, and Lichao Sun. Sora: A review on background, technology, limitations, and opportunities of large vision models, 2024. [3](#)
- [35] Jonathon Luiten, Georgios Kopanas, Bastian Leibe, and Deva Ramanan. Dynamic 3d gaussians: Tracking by persistent dynamic view synthesis. In *3DV*, 2024. [3](#)
- [36] Ben Mildenhall, Pratul P. Srinivasan, Matthew Tancik, Jonathan T. Barron, Ravi Ramamoorthi, and Ren Ng. Nerf: Representing scenes as neural radiance fields for view synthesis. In *ECCV*, 2020. [1](#)
- [37] Linzhan Mou, Jun-Kun Chen, and Yu-Xiong Wang. Instruct 4d-to-4d: Editing 4d scenes as pseudo-3d scenes using 2d diffusion. In *Proceedings of the IEEE/CVF Conference on Computer Vision and Pattern Recognition*, pages 20176–20185, 2024. [1](#), [3](#), [5](#), [6](#), [7](#)
- [38] Thomas Müller, Alex Evans, Christoph Schied, and Alexander Keller. Instant neural graphics primitives with a multiresolution hash encoding. *ACM Trans. Graph.*, 41(4):102:1–102:15, 2022. [4](#)
- [39] Keunhong Park, Utkarsh Sinha, Jonathan T. Barron, Sofien Bouaziz, Dan B Goldman, Steven M. Seitz, and Ricardo Martin-Brualla. Nerfies: Deformable neural radiance fields. *ICCV*, 2021. [2](#)
- [40] William Peebles and Saining Xie. Scalable diffusion models with transformers. In *Proceedings of the IEEE/CVF International Conference on Computer Vision (ICCV)*, pages 4195–4205, 2023. [1](#)
- [41] Ben Poole, Ajay Jain, Jonathan T. Barron, and Ben Mildenhall. Dreamfusion: Text-to-3d using 2d diffusion. In *The Eleventh International Conference on Learning Representations*, 2023. [2](#), [3](#), [4](#), [5](#), [6](#)
- [42] Albert Pumarola, Enric Corona, Gerard Pons-Moll, and Francesc Moreno-Noguer. D-NeRF: Neural Radiance Fields for Dynamic Scenes. In *Proceedings of the IEEE/CVF Conference on Computer Vision and Pattern Recognition*, 2020. [2](#)
- [43] Alec Radford, Jong Wook Kim, Chris Hallacy, Aditya Ramesh, Gabriel Goh, Sandhini Agarwal, Girish Sastry, Amanda Askell, Pamela Mishkin, Jack Clark, Gretchen Krueger, and Ilya Sutskever. Learning transferable visual models from natural language supervision, 2021. [6](#)
- [44] Aditya Ramesh, Prafulla Dhariwal, Alex Nichol, Casey Chu, and Mark Chen. Hierarchical text-conditional image generation with clip latents, 2022. [1](#)
- [45] Jiawei Ren, Liang Pan, Jiaxiang Tang, Chi Zhang, Ang Cao, Gang Zeng, and Ziwei Liu. Dreamgaussian4d: Generative 4d gaussian splatting. *arXiv preprint arXiv:2312.17142*, 2023. [3](#)
- [46] Robin Rombach, Andreas Blattmann, Dominik Lorenz, Patrick Esser, and Björn Ommer. High-resolution image synthesis with latent diffusion models. In *Proceedings of the IEEE/CVF Conference on Computer Vision and Pattern Recognition (CVPR)*, pages 10684–10695, 2022. [1](#), [3](#)
- [47] Nataniel Ruiz, Yuanzhen Li, Varun Jampani, Yael Pritch, Michael Rubinstein, and Kfir Aberman. Dreambooth: Fine tuning text-to-image diffusion models for subject-driven generation. In *Proceedings of the IEEE/CVF Conference on Computer Vision and Pattern Recognition (CVPR)*, pages 22500–22510, 2023. [1](#)
- [48] Ruizhi Shao, Zerong Zheng, Hanzhang Tu, Boning Liu, Hongwen Zhang, and Yebin Liu. Tensor4d: Efficient neural 4d decomposition for high-fidelity dynamic reconstruction and rendering. In *Proceedings of the IEEE Conference on Computer Vision and Pattern Recognition*, 2023. [2](#)
- [49] Ruizhi Shao, Jingxiang Sun, Cheng Peng, Zerong Zheng, Boyao Zhou, Hongwen Zhang, and Yebin Liu. Control4d: Efficient 4d portrait editing with text. 2024. [3](#)
- [50] Yichun Shi, Peng Wang, Jianglong Ye, Long Mai, Kejie Li, and Xiao Yang. MVDream: Multi-view diffusion for 3d generation. In *The Twelfth International Conference on Learning Representations*, 2024. [2](#), [3](#), [5](#), [6](#), [8](#)
- [51] Uriel Singer, Adam Polyak, Thomas Hayes, Xi Yin, Jie An, Songyang Zhang, Qiyuan Hu, Harry Yang, Oron Ashual, Oran Gafni, Devi Parikh, Sonal Gupta, and Yaniv Taigman. Make-a-video: Text-to-video generation without text-video data. In *The Eleventh International Conference on Learning Representations*, 2023. [3](#)
- [52] Liangchen Song, Anpei Chen, Zhong Li, Zhang Chen, Lele Chen, Junsong Yuan, Yi Xu, and Andreas Geiger. Nerfplayer: A streamable dynamic scene representation with decomposed neural radiance fields. *IEEE Transactions on Visualization and Computer Graphics*, 29(5):2732–2742, 2023. [2](#), [6](#)
- [53] Cheng Sun, Min Sun, and Hwann-Tzong Chen. Direct voxel optimization: Super-fast convergence for radiance fields

- reconstruction. In *Proceedings of the IEEE/CVF Conference on Computer Vision and Pattern Recognition (CVPR)*, pages 5459–5469, 2022. 4
- [54] Jiaxiang Tang, Jiawei Ren, Hang Zhou, Ziwei Liu, and Gang Zeng. Dreamgaussian: Generative gaussian splatting for efficient 3d content creation. In *The Twelfth International Conference on Learning Representations*, 2024. 3
- [55] Zachary Teed and Jia Deng. Raft: Recurrent all-pairs field transforms for optical flow (extended abstract). In *Proceedings of the Thirtieth International Joint Conference on Artificial Intelligence, IJCAI-21*, pages 4839–4843. International Joint Conferences on Artificial Intelligence Organization, 2021. Sister Conferences Best Papers. 3, 6
- [56] Edgar Tretschk, Ayush Tewari, Vladislav Golyanik, Michael Zollhöfer, Christoph Lassner, and Christian Theobalt. Non-rigid neural radiance fields: Reconstruction and novel view synthesis of a dynamic scene from monocular video. In *IEEE International Conference on Computer Vision (ICCV)*. IEEE, 2021. 2
- [57] Peng Wang and Yichun Shi. Imagedream: Image-prompt multi-view diffusion for 3d generation. *arXiv preprint arXiv:2312.02201*, 2023. 3
- [58] Zhou Wang, A.C. Bovik, H.R. Sheikh, and E.P. Simoncelli. Image quality assessment: from error visibility to structural similarity. *IEEE Transactions on Image Processing*, 13(4): 600–612, 2004. 6
- [59] Zhengyi Wang, Cheng Lu, Yikai Wang, Fan Bao, Chongxuan Li, Hang Su, and Jun Zhu. Prolificdreamer: High-fidelity and diverse text-to-3d generation with variational score distillation. In *Thirty-seventh Conference on Neural Information Processing Systems*, 2023. 3
- [60] Guanjun Wu, Taoran Yi, Jiemin Fang, Lingxi Xie, Xiaopeng Zhang, Wei Wei, Wenyu Liu, Qi Tian, and Xinggang Wang. 4d gaussian splatting for real-time dynamic scene rendering. In *Proceedings of the IEEE/CVF Conference on Computer Vision and Pattern Recognition (CVPR)*, pages 20310–20320, 2024. 2, 3, 4, 6, 7
- [61] Jay Zhangjie Wu, Yixiao Ge, Xintao Wang, Stan Weixian Lei, Yuchao Gu, Yufei Shi, Wynne Hsu, Ying Shan, Xiaoju Qie, and Mike Zheng Shou. Tune-a-video: One-shot tuning of image diffusion models for text-to-video generation. In *Proceedings of the IEEE/CVF International Conference on Computer Vision*, pages 7623–7633, 2023. 2, 3, 5
- [62] Teng Xu, Jiamin Chen, Peng Chen, Youjia Zhang, Junqing Yu, and Wei Yang. Tiger: Text-instructed 3d gaussian retrieval and coherent editing. *arXiv preprint arXiv:2405.14455*, 2024. 3
- [63] Zeyu Yang, Hongye Yang, Zijie Pan, and Li Zhang. Real-time photorealistic dynamic scene representation and rendering with 4d gaussian splatting. In *International Conference on Learning Representations (ICLR)*, 2024. 2
- [64] Taoran Yi, Jiemin Fang, Junjie Wang, Guanjun Wu, Lingxi Xie, Xiaopeng Zhang, Wenyu Liu, Qi Tian, and Xinggang Wang. Gaussiandreamer: Fast generation from text to 3d gaussians by bridging 2d and 3d diffusion models. In *CVPR*, 2024. 3
- [65] Lvmin Zhang, Anyi Rao, and Maneesh Agrawala. Adding conditional control to text-to-image diffusion models. In *Proceedings of the IEEE/CVF International Conference on Computer Vision (ICCV)*, pages 3836–3847, 2023. 1
- [66] Richard Zhang, Phillip Isola, Alexei A. Efros, Eli Shechtman, and Oliver Wang. The unreasonable effectiveness of deep features as a perceptual metric. In *Proceedings of the IEEE Conference on Computer Vision and Pattern Recognition (CVPR)*, 2018. 6
- [67] Jingyu Zhuang, Chen Wang, Liang Lin, Lingjie Liu, and Guanbin Li. Dreameditor: Text-driven 3d scene editing with neural fields. In *SIGGRAPH Asia 2023 Conference Papers*, New York, NY, USA, 2023. Association for Computing Machinery. 3